Spatial and Temporal Variations of Gravity Wave Parameters. Part I: Intrinsic Frequency, Wavelength, and Vertical Propagation Direction

Ling Wang [1], and Marvin A. Geller

Institute for Terrestrial and Planetary Atmospheres, State University of New York at Stony Brook, Stony Brook, NY 11794-5000

M. Joan Alexander

Colorado Research Associates Division, NorthWest Research Associates, Inc., Boulder, Colorado, 80301

(Submitted to *J. Atmos. Sci.*)

[1]Current affiliation: Colorado Research Associates Division, NorthWest Research Associates, Inc., Boulder, Colorado 80301

Corresponding author address: Ling Wang, Colorado Research Associates Division, NorthWest Research Associates, Inc., 3380, Mitchell Lane Boulder, CO 80301, e-mail: lwang@cora.nwra.com

Abstract

Five years (1998-2002) of U.S. high vertical resolution radiosonde data are analyzed to derive important gravity wave parameters such as intrinsic frequencies, vertical and horizontal wavelengths, and vertical propagation directions in the lower stratosphere and troposphere.

Intrinsic frequencies $\hat{\omega}$ increase with increasing latitude, with larger values in the troposphere. In the lower stratosphere, $\hat{\omega}$ is higher in winter than in summer, especially at mid- and high-latitudes. Intrinsic frequencies divided by the Coriolis parameter f are ~ 4 in the troposphere, and $\sim 2.4 - 3$ in the lower stratosphere. The lower stratospheric $\hat{\omega}/f$ generally decreases weakly with increasing latitude. The latitudinal distributions of the lower stratospheric $\hat{\omega}/f$ are explained largely by the propagation effects. The seasonal variations of $\hat{\omega}$ in the lower stratosphere are found to be related to the variations of the background wind speeds.

Dominant vertical wavelengths decrease with increasing latitude in the lower stratosphere, and maximize at mid-latitudes ($35^\circ - 40^\circ$N) in the troposphere. They are generally longer in winter than in summer. The variations of the dominant vertical wavelengths are found to be associated with the similar variations in gravity wave energies. Dominant horizontal wavelengths decrease with increasing latitude, with larger values in the lower stratosphere.

Approximately 50% of the tropospheric gravity waves show upward energy propagation, whereas there is about 75% upward energy propagation in the lower stratosphere. The lower stratospheric fraction of upward energy propagation is generally smaller in winter than in summer, especially at mid- and high-latitudes. The seasonal variation of upward fraction is likely an artifice due to the analysis method, although

a small part of it may be interpreted by the variations in background wind speeds.

Our results suggest that propagation effects are much more important than source variations for explaining the large-scale time-average properties of waves observed by radiosondes.

1. Introduction

Atmospheric gravity waves play significant roles in the reversal of the temperature gradient at the mesopause and the formation of the warm winter mesopause (Houghton 1978). They also affect the stratospheric temperature distribution and play a role in determining the residual mean meridional circulation via downward control (Haynes et al. 1991; Holton et al. 1995). The effects of gravity waves have to be parameterized or resolved explicitly (which is computationally demanding) in GCM's to obtain realistic mean atmospheric circulations and temperature distributions.

Currently, most GCMs that extend through the middle atmosphere parameterize nonorographic gravity waves by specifying a constant gravity wave source spectrum at a certain altitude. Observational studies, however, have found that gravity wave activity varies significantly both temporally and spatially (Hirota 1984; Fetzer and Gille 1994; Eckermann et al. 1995; Allen and Vincent 1995; Eckermann and Preusse 1999; Tsuda et al. 2000; McLandress et al. 2000; Wang and Geller 2003). For example, Wang and Geller (2003) (hereinafter referred to as WG) derived short vertical wavelength gravity wave energy density morphology from four years (1998-2001) of U.S. radiosonde data. They found the gravity wave variance in these data is stronger in winter than in summer at all latitudes in both the lower stratosphere and troposphere. The variance decreases poleward in the lower stratosphere whereas it maximizes at mid-latitudes ($35° - 40°$N) in the troposphere.

Only recently have a few studies utilized spatially varying gravity wave source spectra in GCM's. Manzini and McFarlane (1998) compared two simulations in which the gravity wave source spectra were launched at two different heights and

had a latitudinal dependence in the characteristic horizontal wavenumber. They found noteworthy differences in the simulated middle atmospheres. Medvedev et al. (1998) showed that an anisotropic source spectrum significantly improves the middle atmosphere circulation compared to an isotropic one. Scaife et al. (2000) specified a gravity wave source spectrum with an enhanced momentum flux in the tropics and obtained a more realistic simulation of the stratospheric quasi-biennial oscillation. McLandress (2002) also found that enhanced rms winds in the tropics resulted in the increased momentum flux that drove the equatorial oscillation.

This paper extends WG by examining wave parameters other than gravity wave energy densities, including intrinsic frequencies, vertical and horizontal wavelengths, and vertical propagation directions from the same but extended data set. It will be shown that all these wave parameters exhibit considerable spatial and temporal variations. The variations can be interpreted by the gravity wave dispersion relation, wave intermittency and energy propagation effects, and/or source characteristics. We try to see which of these effects account for the various observations. In a companion paper, we will show the observations of horizontal propagation directions derived from the data, and investigate the gravity wave source spectra that may give rise to the observed momentum fluxes and wave energies. We believe that such studies can help to specify more realistic gravity wave source spectra for use in GCMs.

The paper is organized as follows: section 2 describes the data and analysis method; section 3 shows the spatial and temporal distributions of gravity wave parameters mentioned above; discussion is given in section 4; in the final section, the summary and conclusions are given.

2. Data and Methods

Data

Five years (1998-2002) of U.S. rawinsonde 6-second resolution data are used in this study. As mentioned in the introduction, the same data set, but with only the first four years of data, has been used in WG to investigate gravity wave energies. Both temperature and horizontal winds are available. For temperature, V*äsälä* RS-80 series ($\sim$ 70% of the stations) and VIZ B2 series ($\sim$ 30% of the stations) radiosondes are used. The accuracy is $\sim 0.2°K$ for the former, and $\sim 0.3°K$ for the latter. The winds are estimated from the elevations and azimuthal angles of the radiosondes which are measured by tracking the position of the balloons using the 6-second Micro-ART system (Williams et al. 1993) for all but one station. The Loran-C windfinding system (NEXUS) is used to determine the wind speeds over Charleston, SC (32.9°N, 280.0°E). The accuracy for the winds is not constant but is generally around 1 ms^{-1} for most of the soundings.

The temperature measurements are recorded at 6-second intervals which correspond to $\sim$ 30 m height resolution, given that the vertical velocity of the balloon is typically $\sim 5\ ms^{-1}$. Smoothing procedures [2] are applied to derive the wind data from the raw elevation and azimuth angle data and the resulting wind data have a vertical resolution of $\sim$150 m. Generally, for each station, roughly half of the soundings are taken at 0000 and 1200 UTCs, respectively.

The location map of stations has been given in WG. As a reference, Table 1

[2]See the *Data Documentation for Data Set Rawinsonde 6-second Data TD6211* (NCDC 2002) for more details about the smoothing.

lists the names and locations of the stations. There are 94 stations in total, located across the contiguous United States, Alaska, Hawaii, Caribbean islands, and western tropical Pacific islands. Since contour maps of wave parameters over the contiguous U.S. will be presented and discussed in this paper, Fig. 1 shows the location map of the radiosonde stations over the contiguous U.S. to help the readers in interpreting the results to be shown in section 3.

Among the stations, four of them (i.e., Corpus Christi, TX, 27.8°N, 262.5°E; Charleston, SC, 32.9°N, 280.0°E; Salt Lake City, UT, 40.8°N, 248.0°E; Guam, Mariana Island, 13.6°N, 144.8°E) miss one or more years of data completely. Also, there is one Southern Hemisphere station, Pago Pago International Airport (14.3°S, 189.3°E) which is located too far away from all the other stations to have it included in the latitudinal mean. Hence, these five stations are excluded completely from the analysis. Since most of the tropospheric soundings over Flagstaff, AZ (35.2°N, 262.6°E) fail to pass the quality control, as will be described later in this section, this station is excluded from the tropospheric analysis. Moreover, the lower stratospheric wind data are believed to be unreliable over Norman, OK (35.2°N, 262.6°E) and Wilmington, OH (39.4°N, 276.3°E) due to low elevation angles and the failure of the Micro-ART system to to lock onto the radiosonde in a timely fashion for the two stations (Miller and Blackmore 1995; Blackmore private communication), so these two stations are excluded from the lower stratospheric analysis. [3]

[3]Since the problems with tracking sondes at low elevation angles are not always appreciated in the literature, we give a brief discussion on the quality of the radiosonde data in the Appendix.

Methods

The analysis methods follow closely Allen and Vincent (1995) and Vincent et al. (1997). Briefly, for each individual soundingprofile, a tropospheric and a lower stratospheric segment are defined for gravity wave analysis. The tropospheric segment is chosen to be 2 to 8.9 km, except for Alaskan stations (thirteen in total) where an altitude range of $2 - 7.4$ km is chosen so as to take proper account of the much lower tropopause in that region. The lower stratospheric segment is specified to be 18 to 24.9 km. Such altitude ranges are very close to what were used in Allen and Vincent (1995). The background Brunt-V*äisälä* frequencies are roughly constant with height over each chosen segment, making the interpretation of the results more straightforward (Allen and Vincent 1995).

Prior to analysis, each raw sounding profile is inspected visually. Those profiles which do not cover the whole altitude range of interest and/or have too many missing records are discarded. Soundings that have suspiciously large gradients in winds and/or temperature are also discarded. Generally, most of the stations have more than 200 valid profiles each year. The station Flagstaff, AZ is a notable exception. There, all of the soundings for the tropospheric segment are discarded because the the station's elevation (2,179 m) is higher than the lowest altitude of the tropospheric segment, and most of the soundings have too large vertical gradient and/or large gaps, especially below 3 km (not shown).

Within each segment, the mean profiles of the zonal and meridional winds and temperature ($\overline{u}, \overline{v}, \overline{T}$) are estimated using second-order polynomial fits. The gravity wave perturbations (u', v', T') are simply the differences between the raw profiles and the mean profiles. Note that linear, second-order, third-order polynomial fits have

been used in earlier studies (e.g., Nastrom et al. 1997, Allen and Vincent 1995, and Vincent et al. 1997, Nastrom and VanZandt 2001). We have tested linear, third-order polynomial, fourth-order polynomial fits and low-pass filter to estimate the background mean profiles, and the analysis results have been compared with the results using the second-order polynomial fit. Separate analyses have also been carried out for soundings taken at 0000 and 1200 UTC, respectively. It is found that the temporal and spatial variations of gravity wave parameters (as will be presented in section 3) remain almost the same for all the different methods tested. In addition, subdivisions of the segments, i.e., $2000 - 5450\ m$, $5450 - 8000\ m$, $18,000 - 21,450\ m$, $21,450 - 24,900\ m$, were also used for alternative analysis to those shown in the next section, and it was found that the major results to be presented in section 3 also remained essentially the same, except for the size of the dominant vertical wavelength (not shown).

For each segment, the segment averaged gravity wave kinetic energy density Ke and potential energy density Pe are estimated using (1) and (2), respectively.

$$Ke = \frac{1}{2}\left(\overline{u'^2} + \overline{v'^2}\right) \tag{1}$$

$$Pe = \frac{g^2}{2N^2}\overline{\hat{T}'^2} \tag{2}$$

where N is the Brunt-V*äisälä* frequency calculated directly from the data; g is the gravitational constant; $\hat{T}' = T'/\overline{T}$ is the normalized temperature fluctuation. The overbar denotes averaging over the segment's altitude range. Note that (1) neglects the vertical velocity contribution to Ke. The segment averaged total gravity wave energy density E_t is simply $Ke + Pe$.

For a monochromatic wave, its intrinsic frequency $\hat{\omega}$, which is the frequency observed in a frame moving in the direction of the background wind, is related with

the axial-ratio of the wind perturbation hodograph, AXR, as follows (Gossard and Hooke 1975; Hines 1989)

$$AXR = \left| \frac{\hat{\omega}}{f} - \frac{1}{N} \frac{dV_T}{dz} \right| \tag{3}$$

where V_T is the mean wind velocity component transverse to the horizontal propagation direction. The readers are referenced to Vincent and Alexander (2000) and Wang et al. (2004) for the determination of horizontal propagation direction. AXR is calculated using the Stokes parameters technique (e.g., Eckermann and Vincent 1989). Note that $\hat{\omega}/f$ larger than certain threshold values cannot be reliably retrieved using (3) (Vincent and Alexander 2000). The threshold $\hat{\omega}/f$ depends on the wind accuracy and rms wave perturbation, with higher wind accuracies and bigger rms wave perturbations leading to larger threshold $\hat{\omega}/f$. To simplify the analysis and to make the results more comparable with previous studies, we exclude $\hat{\omega}$ larger than $10f$ from the computations of the mean $\hat{\omega}$ and horizontal wavelength (the determination of which requires $\hat{\omega}$), as was done in Vincent and Alexander (2000). Since both wind accuracies and rms wave perturbations vary with stations and time, future studies are needed to investigate the effects of varying the threshold $\hat{\omega}/f$ on the analysis results.

The dominant vertical wavenumber $\overline{m}$ is estimated from the "energy-weighted" average vertical wavenumber from the normalized temperature perturbation spectrum. The dominant horizontal wavenumber $\overline{K}$ is determined for each sounding using the gravity wave dispersion relation

$$\overline{K}^2 = \frac{(\overline{m}^2 + \alpha^2)(\hat{\omega}^2 - f^2)}{(N^2 - \hat{\omega}^2)} \tag{4}$$

and using the inferred values of $\hat{\omega}$ and $\overline{m}$. In (4), $\alpha = 1/2H_\rho$ and H_ρ is the density scale height. The dominant vertical wavelength $\overline{\lambda}_z$ and horizontal wavelengths $\overline{\lambda}_h$ are derived from $\overline{m}$ and $\overline{K}$, respectively.

According to linear gravity wave theory, the Coriolis effect causes the perturbation wind vector associated with an upward (downward) propagating gravity wave to rotate anticyclonically (cyclonically) with increasing height (e.g., Holton 1992). The rotary-spectral technique (Vincent 1984) is used to decompose the wind perturbation field into anticlockwise (AW) and clockwise (CW) components. The fraction of upward propagation is simply the ratio of the CW (AW) to ($CW + AW$) in the northern (southern) hemisphere. Note that the above approach tends to underestimate the percentage of upward propagation. It is assumed by the rotary analysis technique that the upward and downward propagating motions are circularly polarized. This assumption leads to decomposing a single upward propagating wave into an upward-propagating fraction of $(1+f/\hat{\omega})/2$, and a downward-propagating fraction of $(1-f/\hat{\omega})/2$ (Vincent 1984; Eckermann and Vincent 1989). When $\hat{\omega}$ is much larger than f, the approach can lead to a significant underestimate of the fraction of upward propagation. As will be shown in section 3, the waves retrieved from the radiosonde flights are mostly low frequency waves with $\hat{\omega}$ about $2-4\ f$. Thus, the discrepancy is not so serious, and meaningful results can still be obtained by this method.

Note that wave parameters are estimated using the linear gravity wave theory in this study. Eckermann and Hocking (1989) cautioned that seemingly "monochromatic" waves can arise naturally from a broad spectrum of waves. The validity of the methods is questionable to some extent when dealing with a spectrum of waves. Note also that our radiosonde analysis can only detect those gravity waves with vertical wavelengths $\leq \sim 7km$. Such a limitation of radiosonde observations must be borne in mind when comparing analysis results from different types of data.

3. Results

In this section, spatial and temporal variations of gravity wave intrinsic frequencies $\hat{\omega}$ scaled by f, vertical and horizontal wavelengths, and fractions of upward energy propagation will be presented. We will show the least processed data, i.e., contour maps of the parameters over the contiguous U.S. first, which are followed by the more processed data, i.e., the zonally averaged result. In the end, the interannual variations of $\hat{\omega}/f$ will be presented.

Fig. 2 shows the contour maps of five-year (1998-2002) averaged December-January-February (DJF), March-April-May (MAM), June-July-August (JJA), and September-October-November (SON) seasonal means of lower stratospheric and tropospheric $\hat{\omega}/f$ over the contiguous U.S. We show $\hat{\omega}/f$ instead of $\hat{\omega}$ because the spatial variations of $\hat{\omega}$ are dominated by f so that other meaningful geographic variations of $\hat{\omega}$ will be obscured if $\hat{\omega}$ itself were shown. The lower stratospheric ratio is generally higher over the east U.S., and smaller over most of the west U.S for all seasons. The ratio generally decreases weakly with increasing latitude except for SON. The tropospheric $\hat{\omega}/f$ is more difficult to characterize, although it is generally higher over part of the Rocky Mountains. Seasonally, the lower stratospheric $\hat{\omega}/f$ is generally higher in winter than in summer. The tropospheric ratio shows much weaker and less coherent seasonal variations. Nevertheless, it is still higher in winter than in summer. $\hat{\omega}$ is generally higher in the troposphere than in the lower stratosphere.

Fig. 3 shows the contour maps of the dominant vertical wavelength $\overline{\lambda}_z$ over the contiguous U.S. In the lower stratosphere, $\overline{\lambda}_z$ is longer over most of the southeast U.S. It is generally shorter over the Rocky Mountains and northwest U.S. In the troposphere, the principal maxima of $\overline{\lambda}_z$ are located over the Rocky Mountains. Seasonally,

$\overline{\lambda}_z$ is generally longer in winter than in summer in both the lower stratosphere and troposphere, except south of $\sim 35\ ^\circ$ where the lower stratospheric $\overline{\lambda}_z$ is actually the longest in summer.

In both the lower stratosphere and troposphere, the geographic distributions of the dominant horizontal wavelength $\overline{\lambda}_h$ over the contiguous U.S. (Fig. 4) are clearly dominated by latitudinal variations, i.e., decreasing with increasing latitude. In the troposphere, secondary features such as relatively longer $\overline{\lambda}_h$ over the east U.S. can also be seen. In the lower stratosphere, $\overline{\lambda}_h$ is longer in summer than in winter over most of the contiguous U.S. There are no coherent seasonal variations of $\overline{\lambda}_h$ in the troposphere.

The geographic distributions of the fraction of upward energy propagation (Fig. 5) are characterized by higher values over the windward side of the Rocky Mountains in the lower stratosphere and over the lee side of the Rocky Mountains in the troposphere. The fraction has a distinctive seasonal cycle in both the lower stratosphere and troposphere, i.e., lower in winter than in summer. Note that, on the average, the fraction is considerably higher in the lower stratosphere than in the troposphere.

The four panels of Fig. 6 show the latitudinal distributions of five-year averaged $\hat{\omega}/f$, $\overline{\lambda}_z$, $\overline{\lambda}_h$, and fraction of upward propagation, respectively. In Fig. 6, each dot represents the mean value of wave parameter over each station. For each station, the monthly means are calculated first. To ensure the representativeness of the monthly means, only those months which have at least 16 valid profiles are included in the calculation of means. The five-year averaged mean value is then calculated from the monthly means from January 1998 to December 2002. The lines in Fig. 6 are the

latitudinal binned results [4] with a bin size of 5°. The black dots and lines are for the lower stratosphere, whereas the red ones are for the troposphere. Compared to the contour maps shown before, information on lower and higher latitudes is also included.

On the average, the lower stratospheric $\hat{\omega}/f$ decreases weakly from ~ 2.8 at 10°N to ~ 2.4 at 65°N. There also exists a local maximum of the ratio at mid-latitudes. As evident from Fig. 2, such a local maximum results from higher values over the east U.S. The tropospheric ratio, on the other hand, displays little latitudinal variations and has a value ~ 4. It is notable that $\hat{\omega}/f$ is higher in the troposphere than in the lower stratosphere by $30 - 60\%$. Since f is a strong function of latitude, Fig. 6 implies that $\hat{\omega}$ actually increases with increasing latitude. In fact, our analysis shows that the intrinsic period decreases from 24.9 hours at 10°N to 5.5 hours at 65°N in the lower stratosphere, and decreases from 17.5 hours at 10°N to 3.3 hours at 65°N in the troposphere.

Distinctive latitudinal patterns of $\overline{\lambda}_z$ can be clearly seen from the upper right panel of Fig. 6. The lower stratospheric $\overline{\lambda}_z$ decreases poleward. The tropospheric $\overline{\lambda}_z$ maximizes at $\sim$ 45°N. It becomes slightly shorter south of 45°N and decreases more rapidly with latitude north of 45°N. Such a sharp decrease of the tropospheric $\overline{\lambda}_z$ from 50°N to 55°N is an artifice caused by the shorter altitude range specified for the Alaskan stations as described in section 2. Because of the shorter altitude range in Alaska, the lowest vertical wavenumber of the waves that can be resolved in the analysis becomes higher than in other regions. Hence, the mean vertical wavelength

[4] As can be seen in Table 1 and Fig. 1 of WG, some latitudes have fewer stations than others. Also, the terrain may differ at some latitudes, so this presentation should be considered for what it is, an average of available station data in certain latitude bands.

will be shorter.

It is evident from the lower left panel of Fig. 6 that $\overline{\lambda}_h$ decreases with increasing latitude in both the lower stratosphere and troposphere. The latitudinal gradient of $\overline{\lambda}_h$, however, is not uniform across the entire latitude range. In both the lower stratosphere and troposphere, $\overline{\lambda}_h$ drops off with latitude very steeply at low-latitudes. The latitudinal gradient becomes much smaller at higher latitudes. It is also worth noting that the lower stratospheric $\overline{\lambda}_h$ is ~ 3 times the tropospheric one throughout the whole latitude range.

The lower right panel of Fig. 6 shows that, in the lower stratosphere, the latitudinal distribution of the fraction of upward propagation shows a weak minimum at mid-latitudes. The tropospheric fraction is slightly higher over Alaska and lower at low latitudes. On the average, $\sim 50\%$ of the gravity wave energy propagates upward in the troposphere, whereas $\sim 75\%$ of the energy propagates upward in the lower stratosphere.

It should be mentioned that the general features of the geographic, seasonal, and latitudinal variations of $\hat{\omega}/f$, $\overline{\lambda}_z$, $\overline{\lambda}_h$, and the fraction of upward propagation as shown in Figs. 2-6 are consistent from year to year, although they do exhibit certain interannual variations, especially for $\hat{\omega}/f$.

Fig. 7 shows the month-latitude contour of the monthly and zonally averaged lower stratospheric $\hat{\omega}/f$. In this figure, the monthly means are calculated first for individual stations. A 5° latitudinal bin is then used to bin the monthly means from different stations into a latitudinal grid from 5°N to 70°N. The interannual variations of $\hat{\omega}/f$ are evident at all latitudes, especially at low latitudes where $\hat{\omega}/f$ is the highest during DJF 1998-99 and 2000-01. Moreover, the latitudinal gradient of the ratio is

notably different during the winter of 1999-2000 than other seasons. Note that WG found that the lower stratospheric total energy density E_t also exhibits considerable interannual variation at low-latitudes, which is related with QBO, i.e., E_t is stronger during the descent of the QBO westerly phase (DJF 1998-99 and 2001-02) and is suppressed during the descent of the QBO easterly phase (DJF 1999-2000 and 2000-01). The interannual variation of $\hat{\omega}/f$, however, does not match the interannual variation of the lower stratospheric E_t. The period of $\hat{\omega}/f$ is $\sim$ two years, whereas the period of E_t is $\sim$ three years (Fig. 11 of WG).

4. Discussion

As shown in section 3, $\hat{\omega}/f$, $\overline{\lambda}_z$, $\overline{\lambda}_h$, and fraction of upward propagation all exhibit certain coherent spatial and temporal variations, especially in the lower stratosphere. It will be demonstrated in this section that most of the observed large scale and seasonal variations can be explained largely by the linear gravity wave dispersion relation, the latitudinal variation in the Coriolis parameter f, and/or background wind Doppler shifting. The lower stratospheric results are influenced a great deal by vertical energy propagation considerations. Source information is more easily seen in the troposphere. Perhaps then, specification of gravity wave sources in the troposphere may not be so important for the parameterization of low intrinsic frequency middle atmosphere gravity wave effects in global circulation models since propagation effects seem to dominate for these waves in the radiosonde observations.

4.1 Intrinsic Frequency $\hat{\omega}$ and $\hat{\omega}/f$

Note that the maximum vertical wavelength that can be resolved in our analysis is 6.9 km, whereas the horizontal wavelength is at least hundreds of kilometers (see Fig. 6). This implies that $\overline{m} \gg \overline{K}$ and $\overline{m} \gg \alpha$. Hence, (4) is reduced to

$$\hat{\omega}^2 - f^2 = N^2 \overline{K}^2 / \overline{m}^2 \tag{5}$$

Since N and $\overline{m}$ are not as strong functions of latitude as f is (Fig. 6), (5) indicates that both $\hat{\omega}$ and $\overline{K}$ (or $1/\overline{\lambda}_h$) vary approximately linearly with f, as indeed shown in the upper right and lower right panels of Fig. 6, respectively.

The derived $\hat{\omega}$ are generally very low, being around $4f$ in the troposphere and $2.4 - 3$ f in the lower stratosphere (Figs. 2 and 6). In fact, low intrinsic frequency

gravity waves were also identified in previous analyses of radiosonde and rocket soundings (e.g., Hamilton 1991; Eckermann et al. 1995; Vincent et al 1997; Vincent and Alexander 2000). For example, in analyzing six years of radiosonde soundings over Cocos Islands, Vincent and Alexander (2000) found that the motion field appeared to be dominated by waves with frequencies of $2.7f$ in the lower stratosphere. The tendency for observing low $\hat{\omega}$ waves in radiosonde and rocket soundings may be in part due to the fact that these observational techniques can only detect relatively short vertical wavelength waves. Given the same horizontal wavelength, shorter vertical wavelengths lead to lower $\hat{\omega}$, as suggested by (5). The tendency for observing low $\hat{\omega}$ waves may also be explained in part by the gravity wave vertical group velocity effect. The gravity wave vertical group velocity c_{gz} is given by

$$c_{gz} = -\frac{\hat{\omega}^2 - f^2}{\hat{\omega} m \left(1 + \frac{\hat{\omega}^2 - f^2}{N^2 - \hat{\omega}^2}\right)} \simeq -\frac{\hat{\omega}^2 - f^2}{\hat{\omega} m} \tag{6}$$

which implies that waves of higher $\hat{\omega}$ have larger c_{gz}, and thus their energies move faster through a given altitude region. Fig. 8 shows the propagation time versus latitude for different $\hat{\omega}$. In this plot, the propagation time is the time it would take a wave of a given $\hat{\omega}$ and a vertical wavelength of 2.5 km to travel vertically through a 7-km-deep layer in the lower stratosphere. A typical lower stratospheric value of 0.02 s^{-1} is used for N to calculate the propagation time. It is evident from Fig. 8 that the propagation time depends strongly on $\hat{\omega}$. The lower the $\hat{\omega}$, the longer it takes a wave to propagate through a given vertical distance. Note that the temporal sampling of radiosonde observations is only twice daily, so radiosondes are more capable of capturing the slowly moving low $\hat{\omega}$ waves, if there is intermittency in the wave sources (as can be expected for convection generated waves for instance). Since low $\hat{\omega}$ waves are more likely to be observed by radiosondes, and since f defines the lowest $\hat{\omega}$ for

gravity waves, it follows that the average $\hat{\omega}$ in these observations should show a strong dependence on f (Alexander et al. 2002).

In the lower stratosphere, the five-year averaged $\hat{\omega}/f$ decreases weakly poleward (Fig. 6). Similar but larger latitudinal variations of $\hat{\omega}/f$ have also been observed from CRISTA data (Preusse, private communication) and rocket observations (e.g., Hirota and Niki 1985). For example, Hirota and Niki (1985) found that in the altitude range of $30-60$ km, $\hat{\omega}/f$ was in the range of $2.5-5$ and decreased with increasing latitude. Note that in their study, fluctuations with vertical scales between 1 and 15 km were obtained from rocket observations. The inclusion of larger vertical scale of motions in their study may explain the larger value of $\hat{\omega}/f$ than ours, as implied by (5).

The latitudinal variations of the lower stratospheric $\hat{\omega}/f$ may also be explained conceptually by the vertical group velocity effect. Fig. 8 shows clearly that the vertical propagation time of a wave with a given $\hat{\omega}$ decreases with increasing latitude. At lower latitudes, radiosondes not only detect the very low $\hat{\omega}/f$ waves, they are also capable of capturing some higher $\hat{\omega}/f$ waves because at low latitudes, some higher $\hat{\omega}/f$ waves propagate slowly enough in the vertical for them to be well sampled by radiosondes. At higher latitudes, on the other hand, only the very low $\hat{\omega}/f$ waves propagate slow enough for the temporal sampling of radiosondes. This may explain why the averaged $\hat{\omega}/f$ decreases with increasing latitude. Of course, the latitudinal distribution of $\hat{\omega}/f$ can be complicated by the variations of wave intermittency, background winds, and characteristics of different types of wave sources. These factors may lead to the localized maximum of the lower stratospheric $\hat{\omega}/f$ at mid-latitudes caused by higher $\hat{\omega}$ over the east U.S. (Figs. 2 and 6).

The larger values of $\hat{\omega}/f$ in the lower stratosphere at high-latitudes during DJF

1999-2000 (Fig. 7) is probably related to the exceptionally strong background winds in that region during that time. Fig. 9 shows the month-altitude contour of the monthly mean background wind speeds over Point Barrow, AK (71.3°N, 203.2°E) from the U.S. radiosondes. The wind speeds have been smoothed in the vertical. It is obvious that the wind is the strongest, exceeding 60 ms^{-1} in the lower stratosphere, during the winter of 1999-2000. Wind speeds over most of the other Alaskan stations display the similar features (not shown). The especially strong lower stratospheric winds during DJF 1999-2000 act to Doppler shift waves propagating upstream to higher $\hat{\omega}$, and hence are responsible for the higher values of $\hat{\omega}/f$ during DJF 1999-2000. This also implies that most waves propagate westward (i.e., opposite to winds) in that region and during that time. In a companion paper (Wang et al. 2004), it will be shown that waves indeed propagate roughly opposite to the background winds in the lower stratosphere.

The higher $\hat{\omega}$ in the troposphere than in the lower stratosphere (Figs. 2 and 6) may be related to the fact that most gravity wave sources are located in the troposphere so that the considerations of vertical energy propagation are less important compared with the lower stratosphere. It is unclear at the moment what is (are) the exact cause(s) for this troposphere-lower stratosphere difference in $\hat{\omega}$.

The seasonal variations of the lower stratospheric $\hat{\omega}/f$ at mid-latitudes (Fig. 2), i.e., higher values in winter than in summer, may be explained by the seasonal variations of the background winds. The upper left panel of Fig. 10 shows the monthly time series of the monthly and zonally averaged $\hat{\omega}/f$ (thick solid lines) and background wind speeds from the radiosondes averaged over $18 - 24.9$ km (thick dotted lines) in the lower stratosphere at different latitudes ($10° - 70°$N). The correlations be-

tween $\hat{\omega}/f$ and wind speeds are high and positive at mid- and high-latitudes. Though smaller, the correlation is also significant at 95% confidence level at 10°N. The correlation is positive but insignificant at 30°N. Stronger background winds in winter generally tend to Doppler shift waves propagating against the winds to higher $\hat{\omega}$, so the annual cycle of the lower stratosphe ric $\hat{\omega}/f$ is likely caused by the temporal variations of the backgrou nd wind speeds via the Doppler shift effect. Indeed, the correlation between the monthly time series of $\hat{\omega}/f$ and that of the background wind speed has also been calculated for each individual station (not shown). Positive and significant correlations can be obtained for more than two-thirds of the total stations for the lower stratospheric segment. Best correlations are generally seen for stations located at mid- and high-latitudes (north of 40°N). Lower but still significant correlations are seen for most of the tropical stations. These provide strong evidence that the temporal variations of $\hat{\omega}/f$ are related with that of the background wind speeds. The correlation is generally poor for stations located between 15° and 35°N. In general, the correlation is insignificant for the tropospheric segment.

Vertical Wavelength

As mentioned before, the vertical wavelengths that can be resolved in this study are severely limited by the vertical scale of radiosonde observations and the analysis method used, thus only relatively short vertical wavelength waves can be reliably retrieved from the U.S. radiosonde soundings.

It is interesting that the latitudinal distribution of the dominant vertical wavelength $\overline{\lambda}_z$ (the upper right panel of Fig. 6) resembles that of the gravity wave total energy density E_t (Fig. 4 of WG). They both maximize at mid-latitudes in the tro-

posphere and decrease with increasing latitude in the lower stratosphere. In fact, the latitudinal distributions of both the potential energy density Pe and kinetic energy density Ke (not shown) are also quite similar to those of E_t and $\overline{\lambda}_z$. The seemingly good correspondence between the latitudinal distribution of $\overline{\lambda}_z$ and gravity wave energy density can be explained schematically by Fig. 11 which shows two vertical wavenumber power spectra of gravity wave perturbations with energies of E_1 (solid curve) and E_2 (dashed curve), respectively, in energy-conservation coordinates. According to wave saturation theory, the tail (saturated) parts of the two spectra should have the same intensity if the Brunt-V*äisälä* frequency is assumed to be the same. It follows then that the energy-weighted vertical wavenumber for the solid curve should be smaller than that for the dashed curve. In other words, there should be a positive correlation between gravity wave energy and the energy-weighted vertical wavelength.

The seasonal variations of $\overline{\lambda}_z$ (Fig. 3) may also be related to gravity wave energies. WG showed that E_t are generally larger in winter than in summer in both the lower stratosphere and troposphere. It follows from Fig. 11 that $\overline{\lambda}_z$ should also be longer in winter than in summer in both regions. The upper right panel of Fig. 10 shows that the monthly time series of $\overline{\lambda}_z$ and Pe are indeed positively and significantly correlated, except at 30°N in the lower stratosphere. Note that the seasonal variations of gravity wave energies may be related with the seasonal variations of the density and stability of the background atmosphere (Eckermann 1995). The argument illustrated in Fig. 11 can also be applied to explain the longer vertical wavelengths over the Rocky Mountains in the troposphere (cf. Fig. 5 of WG.)

Fig. 10 indicates that the seasonal variations of the lower stratospheric $\hat{\omega}/f$, $\overline{\lambda}_z$, and wind speeds are quite similar. This is understandable since the dispersion relation

(5) implies that seasonal changes in winds could give positive correlations between $\overline{\lambda}_z$ and $\hat{\omega}/f$ for constant N and $\overline{\lambda}_h$. Correlations between $\overline{\lambda}_z$ and $\hat{\omega}/f$ are good over Rocky Mountain stations, but generally poor elsewhere, suggesting other factors are also important.

Horizontal Wavelength

As mentioned in the introduction, Manzini and McFarlane (1998) introduced a latitudinal dependence in their characteristic horizontal wavelength of the gravity wave source spectrum. Their characteristic horizontal wavelength was specified to decrease from around 700 km at 10°N to around 300 km at 65°N. The latitudinal pattern of their horizontal wavelengths agrees with our results although the exact values are not the same. The latitudinal distribution of $\overline{\lambda}_h$ has been interpreted in the subsection on $\hat{\omega}$ earlier in this section by the simplified dispersion relation (5). Troposphere-stratosphere differences in $\overline{\lambda}_h$ are mainly due to larger values of N in the lower stratosphere than in the troposphere. On the average, the ratio of the lower stratospheric to the tropospheric N is ~ 2, while the ratio of the lower stratospheric to the tropospheric $\overline{\lambda}_h$ is ~ 3 (Figs. 4 and 6). Hence, about one third of the differences are caused by other factors.

According to (5), $\overline{\lambda}_h$ should be proportional to N and $\overline{\lambda}_z$, and inversely proportional to $\hat{\omega}/f$. Fig. 10 show that the seasonal variations of $\overline{\lambda}_h$ are indeed positively correlated with N and negatively correlated with $\hat{\omega}/f$ at mid-latitudes (e.g., 40°N), but they are negatively correlated with $\overline{\lambda}_z$. This indicates that N and $\hat{\omega}$ dominate the seasonal variations of $\overline{\lambda}_h$, whereas the effect of $\overline{\lambda}_z$ on $\overline{\lambda}_h$ is negligible at mid-latitudes. Note that the consistency among $\overline{\lambda}_h$, $\overline{\lambda}_z$, $\hat{\omega}/f$ and N should be expected since $\overline{\lambda}_h$ is

derived from the other parameters using the gravity wave dispersion relation (4).

Vertical Propagation Direction

On the average, 50% wave energies propagate upward in the troposphere, whereas 75% wave energies propagate upward in the lower stratosphere. This indicates that some waves might be generated in the upper troposphere and/or that tropospheric reflections of gravity waves are occurring. Similar troposphere-stratosphere differences were also obtained by earlier studies. For example, Vincent et al. (1997) found that typically $60 - 80\%$ of the wave energies propagate upward over Macquarie Island in the lower stratosphere. Eckermann et al. (1995) examined the rocket data in the $20 - 60$ km altitude range and found that the fraction was more than 50% in the lower stratosphere.

Distinctive seasonal variations of the fraction of upward propagation have been found from the U.S. radiosonde observations. Temporal variations of fraction of upward propagation have also been reported in previous studies. Zink and Vincent (2001) analyzed radiosonde soundings over Macquarie Island (55°S, 159°E) and found that the amount of wave energy propagating upward minimized in winter, consistent with our results. Eckermann et al. (1995), on the other hand, found that the percentage of upward propagation showed a marked semi-annual variation in the rocket data, with equinoctial maxima and minima at the solstices. In addition, they found that the winter minimum was almost always deeper than the summer one.

Zink and Vincent (2001) explained the winter minimum and summer maximum of the fraction in their data by the seasonal variations of the background wind speeds. They argued that the stronger winds over Macquarie Island in winter tend to Doppler

shift a gravity wave propagating against the wind to a higher $\hat{\omega}$. When its intrinsic frequency reaches the reflection frequency (which is generally close to N, but can be considerably lower than N for long horizontal wavelength waves), the wave's vertical group velocity will change sign and the wave will be reflected. Thus, the fraction of upward propagation is smaller in winter, and there should be a negative correlation between the percentage of upward propagation and the strength of the background winds.

Such a negative relationship between the fraction and the background wind speeds is also seen in the U.S. radiosonde observations. The lower right panel of Fig. 10 compares the monthly time series of the fraction with that of the background wind speeds in the lower stratosphere. It is evident that the two are negatively and significantly correlated for all the latitudinal bands except at 30°N, suggesting that the seasonal variations of the fraction may be related to the seasonal variations of the background winds. It should be borne in mind that only those very short waves (with horizontal wavelengths of several tens of kilometers or less) are likely to be Doppler shifted to their reflection frequencies, the Doppler shift and wave reflection argument therefore can only explain a small part of the seasonal variations of the fraction of upward propagation, especially at lower latitudes where the dominant horizontal wavelengths are $\sim 1000\ km$ or longer (Fig., 6).

Fig. 10 also shows that the seasonal variation of the upward fraction is significantly and negatively correlated with that of $\hat{\omega}$ throughout the latitudinal range ($10°-70°$N). In fact, their correlation coefficient (not shown) is higher than that between the upward fraction and wind speeds, especially at 30°N, and the coefficient is smaller at higher latitudes than at lower latitudes. As mentioned in section 2, the rotary spectral

analysis technique decomposes a single upward propagating wave into both upward and downward propagating parts with the upward part given only $(1 + f/\hat{\omega})/2$ of the true amplitude. Hence, the calculated fraction will be inversely correlated with $\hat{\omega}$ even when the true fraction remains a constant (see Fig. 10). So, the seasonal variation of the fraction of upward propagation is most likely an artifice caused by the rotary spectral analysis method, although a small part of it may be caused by the variations in background wind speeds, as discussed above. It remains to be investigated to what extent the temporal variations of the calculated fraction of upward propagation reflect the temporal variations of the real fraction.

In the lower stratosphere, the particularly small value of fraction at high latitudes (north of 50°N) during DJF 1999-2000 (the lower right panel of Fig. 10) may be associated with the exceptionally strong background winds in that region and during that time (e.g., Fig. 9). It may also be an artifice due to the corresponding exceptionally high frequency (Fig. 7).

In addition to propagation considerations, there are also gravity wave sources inside the troposphere and the sources will most likely vary with time. Thus, the temporal variations of the fraction of upward gravity wave energy propagation is more complicated in the troposphere, as shown in the lower right panel of Fig. 10. Note that the higher fractions over the Rocky Mountains in the troposphere (Fig. 5) are consistent with topography being the major source of gravity waves over that region. Over other regions, gravity wave sources may probably be located at higher levels.

5. Summary and Conclusions

Atmospheric gravity wave information has been derived from five years (1998-2002) of high vertical resolution U.S. radiosonde data over almost 90 stations. For each of the soundings, a tropospheric and lower stratospheric segment are selected for gravity wave analysis. Within each segment, gravity wave perturbations are estimated by subtracting a second-order polynomial fit from the original sounding. The derived wind and temperature perturbations are used to estimate gravity wave parameters such as the intrinsic frequency, the vertical and horizontal wavelengths, and the direction of vertical energy propagation. Distinctive spatial and temporal variations of these parameters have been found.

Consistent with previous studies, the dominant gravity wave intrinsic frequency increases with increasing latitude in both the troposphere and lower stratosphere. This result is interpreted in terms of the gravity wave dispersion relation. Also, the lower stratospheric frequency is systematically less than the tropospheric one. This is a new result from our study, and the reason(s) for this troposphere-stratosphere is (are) unknown at the moment. In the lower stratosphere, the intrinsic frequency is higher in winter and lower in summer, especially at mid- and high-latitudes. This is also a new result from our study, and is interpreted by the temporal variations of winds via the Doppler shift effect.

The dominant intrinsic frequency divided by f has values around 4 in the troposphere, and $2.4-3$ in the lower stratosphere. Such low intrinsic frequency waves were also identified in previous studies of radiosondes and rocket soundings. The tendency to observe low intrinsic frequency waves is likely caused by the fact that radiosondes can only detect relatively short vertical wavelength waves which have low intrinsic

frequencies and by the limitation of the temporal sampling of radiosondes. In the lower stratosphere, $\hat{\omega}/f$ generally decreases weakly with increasing latitude. Such a latitudinal variation of $\hat{\omega}/f$ is consistent with the results of previous studies, and may be related to the gravity wave vertical group velocity effect and may also be related with the limitation of the temporal sampling of radiosondes.

The dominant vertical wavelength decreases with increasing latitude in the lower stratosphere, and maximizes at mid-latitudes ($35^\circ - 40^\circ$N) in the troposphere. In both the troposphere and lower stratosphere, the vertical wavelengths are longer in winter than in summer. These are new results from our study. The latitudinal and seasonal variations of vertical wavelengths are consistent with the variations of the gravity wave energy density from gravity wave saturation theory.

The dominant horizontal wavelength decreases with increasing latitude in both the troposphere and lower stratosphere, with larger values in the lower stratosphere. The latitudinal variation of horizontal wavelength is consistent with previous studies, and is shown to be a straightforward result of the gravity wave dispersion relation. The troposphere-stratosphere differences are caused mostly by the differences in the stability characteristics in the two different regions.

Approximately 50% of the tropospheric gravity waves show upward energy propagation, whereas there is about 75% upward propagation in the lower stratosphere, indicating that some waves might be generated in the upper troposphere and/or that tropospheric reflections of gravity waves are occurring. This is consistent with previous studies. The lower stratospheric percentage is generally smaller in winter and higher in summer, especially at mid- and high-latitudes. Such seasonal variations are likely artifices caused by the seasonal variations in $\hat{\omega}$ and errors in the rotary analysis

technique that are proportional to $\hat{\omega}$. A small part of the seasonal variations may also be interpreted in terms of stronger winds in winter which leads to more occurrences of wave reflection and weaker winds in summer resulting in less wave reflection (Zink and Vincent 2001).

As a critical note on the derived morphology of gravity wave parameters, it should be borne in mind that gravity waves have a wide spectrum, but radiosondes can only detect part of the spectrum, i.e., low intrinsic frequency and short vertical wavelength. The combination of the so called "observational filter" effect (Alexander 1998) and the propagation of waves in the atmosphere renders the interpretation of the derived morphology of gravity wave activity in terms of wave sources less straightforward. Also, we should be aware of the limit of the gravity wave analysis method used in this study. Many of the wave parameters are derived using the dispersion and polarization relations for a linear monochromatic wave. Hence, the analysis results are compromised in cases when we are dealing with a superposition of waves. In addition, it is questionable whether the second-order polynomial fits truly represent the background fields in the troposphere where it is difficult to separate the perturbations caused by gravity waves from those caused by temperature inversions and frontal systems.

Nevertheless, the morphology of wave parameters derived from this study is helpful in specifying gravity wave source spectra for use in GCMS. In particular, our results suggest that specifying the physical sources in the lower troposphere may not be so important for low frequency waves. The propagation effects appear to dominate to a very large extent. Furthermore, Alexander and Vincent (2000) and a companion paper (Wang et al. 2004) both imply that best fits of wave energies and momentum fluxes are obtained with source specifications in the upper troposphere.

Acknowledgments

The authors would like to thank Drs. Robert A. Vincent, Valery A. Yudin, and Steven D. Eckermann for helpful discussions with them regarding this paper. We would also like to thank the editor and the three anonymous reviewers for their very constructive comments that result in a much improved paper. This research was funded by the U.S. National Science Foundation under grant ATM-1011039, Award 10447. M. J. Alexander's work was funded by the National Science Foundation Grant No. 0234230 and NASA ACMAP contract NASW-01017.

APPENDIX – Data Quality

The U.S. radiosonde network wind soundings are measured by the Micro-ART (Micro computer Automated Radio Theodolite) system for most of the stations. Micro-ART utilizes a radio direction finding (RDF) antenna linked to a personal computer to record six second measurements of the azimuth and elevation angle of the radiosonde flight train. Details of the methods used to retrieve winds from the measurements of the azimuth and elevation angles can be found in the *Micro-ART Observation and Rework Programs Technical Document (NWS 1991)* and the *Data Documentation for Data Set Rawinsonde 6-second Data TD6211* (NCDC 2002).

Williams et al. (1993) and Miller and Blackmore (1995) noted that the data quality of the six-second winds in the lower stratosphere deteriorates when the following instrument related problems occurs: (1) the elevation angles approach the elevation angle limit; and (2) the Micro-ART system fails to lock onto the radiosonde in a timely fashion so that spurious oscillations occur. The elevation angle problem is more serious in winter when the background wind is strong so that the elevation angle is generally low and is close to the elevation angle limit (normally 6°). Blackmore (private communication) also noted that two stations, i.e., Norman, OK and Wilmington, OH, are particularly susceptible to the above problems.

To minimize the effect of data noise, for future work, we need to develop proper smoothing algorithms to filter out abnormally high level of noise in some of the lower stratospheric wind profiles and to extract as much geophysical information as possible and to minimize the noise contributions.

References

[1] Alexander, M. J., 1998: Interpretations of observed climatological patterns in stratospheric gravity wave variance, *J. Geophys. Res.,* **103,** 8627-8640.

[2] —, and R. A. Vincent, 2000: Gravity waves in the tropical lower stratosphere: A model study of seasonal and interannual variability, *J. Geophys. Res.,* **105,** 17 983-17 993.

[3] —, T. Tsuda, and R. A. Vincent, 2002: Latitudinal variations observed in gravity waves with short vertical wavelengths. *J. Atmos. Sci.,* **59,** 1394-1404.

[4] Allen, S., and R. A. Vincent, 1995: Gravity wave activity in the lower atmosphere: Seasonal and latitudinal variations, *J. Geophys. Res.,* **100,** 1327-1350.

[5] Eckermann, S. D., and R. A. Vincent, 1989: Falling sphere observations of anisotropic gravity wave motions in the upper stratosphere over Australia. *Pure Appl. Geophys.,* **130,** 509-532.

[6] —, and W. K. Hocking, 1989: Effect of superposition on measurements of atmospheric gravity waves: A cautionary note and some reinterpretations. *J. Geophys. Res.,* **94,** 6333-6339.

[7] —, I. Hirota, and W. K. Hocking, 1995: Gravity wave and equatorial wave morphology of the stratosphere derived from long-term rocket soundings. *Q. J. R. Meteorol. Soc.,* **121,** 149-186.

[8] —, 1995: On the observed morphology of gravity-wave and equatorial-wave variance in the stratosphere. *J. Atmos. Terr. Phys.,* **57,** 105-134.

[9] —, and P. Preusse, 1999: Global measurements of stratospheric mountain waves from space. *Science,* **286**, 1534-1537.

[10] Fetzer, E. J., and J. C. Gille, 1994: Gravity wave variance in LIMS temperatures. Part I: Variability and comparison with background winds. *J. Atmos. Sci.,* **53,** 398-410.

[11] Gossard, E. E., and W. H. Hooke, 1975: *Waves in the Atmosphere*, Elsevier Science, New York.

[12] Hamilton, K., 1991: Climatological statistics of stratospheric inertia-gravity waves deduced from historical rocketsonde wind and temperature data, *J. Geophys. Res.,* **96,** 20 831-20 829.

[13] Haynes, P. H., C. J. Marks, M. E. McIntyre, T. G. Shepherd, and K. P. Shine, 1991: On the "downward control" of extratropical diabatic circulations by eddy-induced mean zonal forces, *J. Atmos. Sci.,* **48,** 651-678.

[14] Hines, C. O., 1989: Tropopausal mountain waves over Arecibo: A case study, *J. Atmos. Sci.,* **46,** 476-488.

[15] Hirota, I., 1984: Climatology of gravity waves in the middle atmosphere, *J. Atmos. Terr. Phys.,* **46,** 767-773.

[16] —, and T. Niki, 1985: A statistical study of inertia-gravity waves in the middle atmosphere. *J. Meteorol. Soc. Jpn,* **63,** 1055-1066.

[17] Holton, J. R., 1992: An Introduction to Dynamic Meteorology. *Academic Press,* 3rd ed. San Diego, 507 pp.

[18] —, P. H. Haynes, M. E. McIntyre, A. R. Douglass, R. B. Rood, and L. Pfister, 1995: Stratosphere-troposphere exchange, *Rev. Geophys.,* **33,** 403-439.

[19] Houghton, J. T., 1978: The Stratosphere and Mesosphere, *Q. J. Roy. Meteor. Soc.,* **104,** 1-29.

[20] Manzini, E., and N. McFarlane, 1998: The effect of varying the source spectrum of a gravity wave parameterization in a middle atmosphere general circulation model. *J. Geophys. Res.,* **103,** 31 523-31 539.

[21] McLandress, C., M. J. Alexander, and D. L. Wu, 2000: Microwave Limb Sounder observations of gravity waves in the stratosphere: A climatology and interpretation, *J. Geophys. Res.,* **105,** 11,947-11967.

[22] —, 2002: Interannual variations of the dirunal tide in the mesosphere induced by a zonal-mean wind oscillation in the tropics. *Geophys. Res. Lett.,* **29,** 10.1029/2001GL014551.

[23] Medvedev, A., G. Klaassen, and S. Beagley, 1998: On the role of an anisotropic gravity wave spectrum in maintaining the circulation of the middle atmosphere. *Geophys. Res. Lett.,* **25,** 509-512.

[24] Miller, E., and W. Blackmore, 1995: A comparison of radiosonde windfinding techniques: Micro-ART and NEXUS (Loran-C Radionavigation). Preprints, *Ninth Symposium on Meteorological Observations and Instrumentation,* Charlotte, NC, Amer. Meteor. Soc., 49-54.

[25] Nastrom, G. D., T. E. VanZandt, and J. M. Warnock, 1997: Vertical wavenumber spectra of wind and temperature from high-resolution balloon soundings in the lower atmosphere over Illinois. *J. Geophys. Res.,* **102**, 6685- 6702.

[26] Nastrom, G. D., and T. E. VanzZandt, 2001: Seasonal variability of the observed vertical wave number spectra of wind and temperature and the effects of prewhitening. *J. Geophys. Res.,* **106,** 14,369-14,375.

[27] Scaife, A., N. Butchart, C. Warner, D. Stainforth, and W. Norton, 2000: Realistic quasi-biennial oscillations in a simulation of the global climate. *Geophys. Res. Lett.,* **27,** 3481-3484.

[28] Tsuda, T., M. Nishida, C. Rocken, and R. H. Ware, 2000: A global morphology of gravity wave activity in the stratosphere revealed by the GPS occultation data (GPS/MET), *J. Geophys. Res.,* **105,** 7257-7274.

[29] Vincent, R. A., 1984: Gravity-wave motions in the mesosphere. *J. Atmos. Terr. Phys.,* **46,** 119-128.

[30] —, S. J. Allen, and S. D. Eckermann, 1997: Gravity-wave parameters in the lower stratosphere. *Gravity Wave Processes: Their Parameterization in Global Climate Models,* K. Hamilton, Ed., Springer-Verlag, 7-25.

[31] —, and M. J. Alexander, 2000: An observational study of seasonal and interannual variability, *J. Geophys. Res.,* **105,** 17 971-17 982.

[32] Wang, L., and M. A. Geller, 2003: Morphology of Gravity Wave Energy as Observed from Four Years (1998-2001) of High Vertical Resolution U.S. Radiosonde Data, *J. Geophys. Res.,* **108,**, 10.1029/2002JD002786.

[33] Wang, L., M. A. Geller, and M. Joan Alexander, 2004: Spatial and temporal variations of gravity wave parameters. Part II: Horizontal propagation directions and gravity wave source spectra, to be submitted.

[34] Williams, S. F., C. G. Wade, and C. Morel, 1993: A comparison of high resolution radiosonde winds: 6-second Micro-ART winds versus 10-second CLASS LORAN winds. Preprints, *Eighth Symposium on Meteorological Observations and Instrumentation,* Anaheim, California, Amer. Meteor. Soc., 60-65.

[35] Zink, F., and R. A. Vincent, 2001: Wavelet analysis of stratospheric gravity wave packets over Macquarie Island 1. Wave parameters. *J. Geophys. Res.,* **106**, 10,275-10,288.

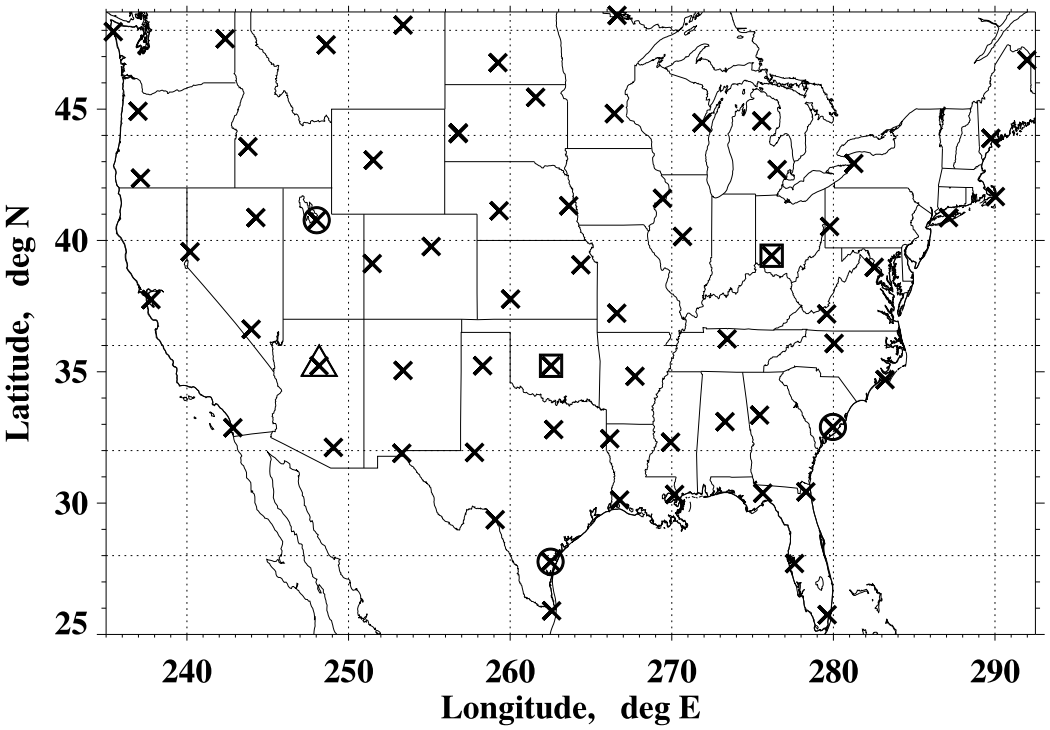

Fig. 1: Location map of the U.S. stations over the contiguous U.S. Stations that are not included in this analyses at all are circled. Stations that are excluded from the lower stratospheric analysis only are denoted by open squares. The station that is excluded from tropospheric analysis only is denoted by a triangle. See text for details.

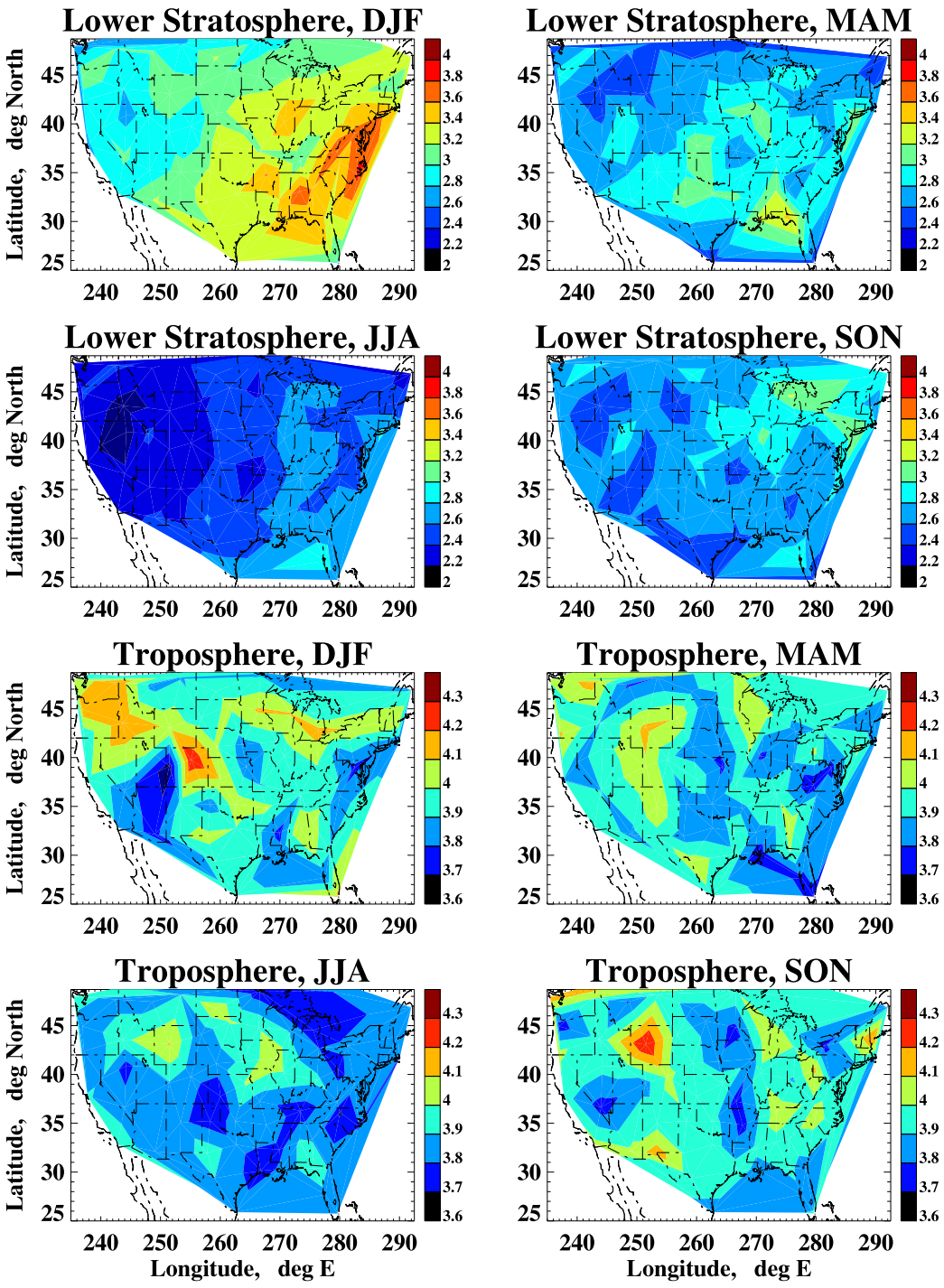

Fig. 2: Contoured maps of five-year (1998-2002) averaged seasonal means (DJF, MAM, JJA, and SON) of lower stratospheric and tropospheric intrinsic frequencies divided by the Coriolis parameter, $\hat{\omega}/f$, over the contiguous United States. The contour interval is 0.2 for the lower stratosphere and 0.1 for the troposphere.

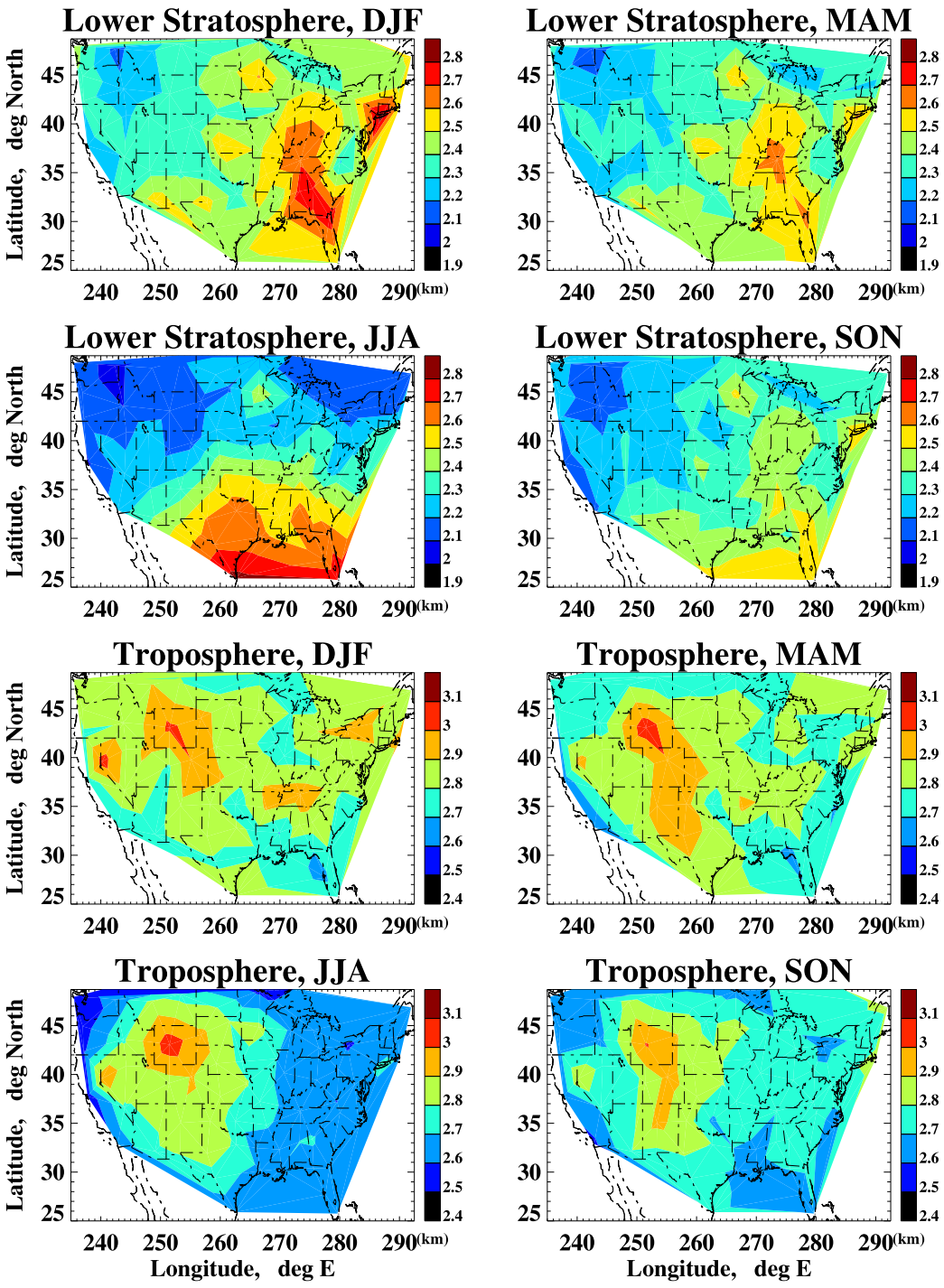

Fig. 3: Same as Fig. 2 but for the dominant vertical wavelength $\overline{\lambda}_z$. The contour interval is 0.1 km.

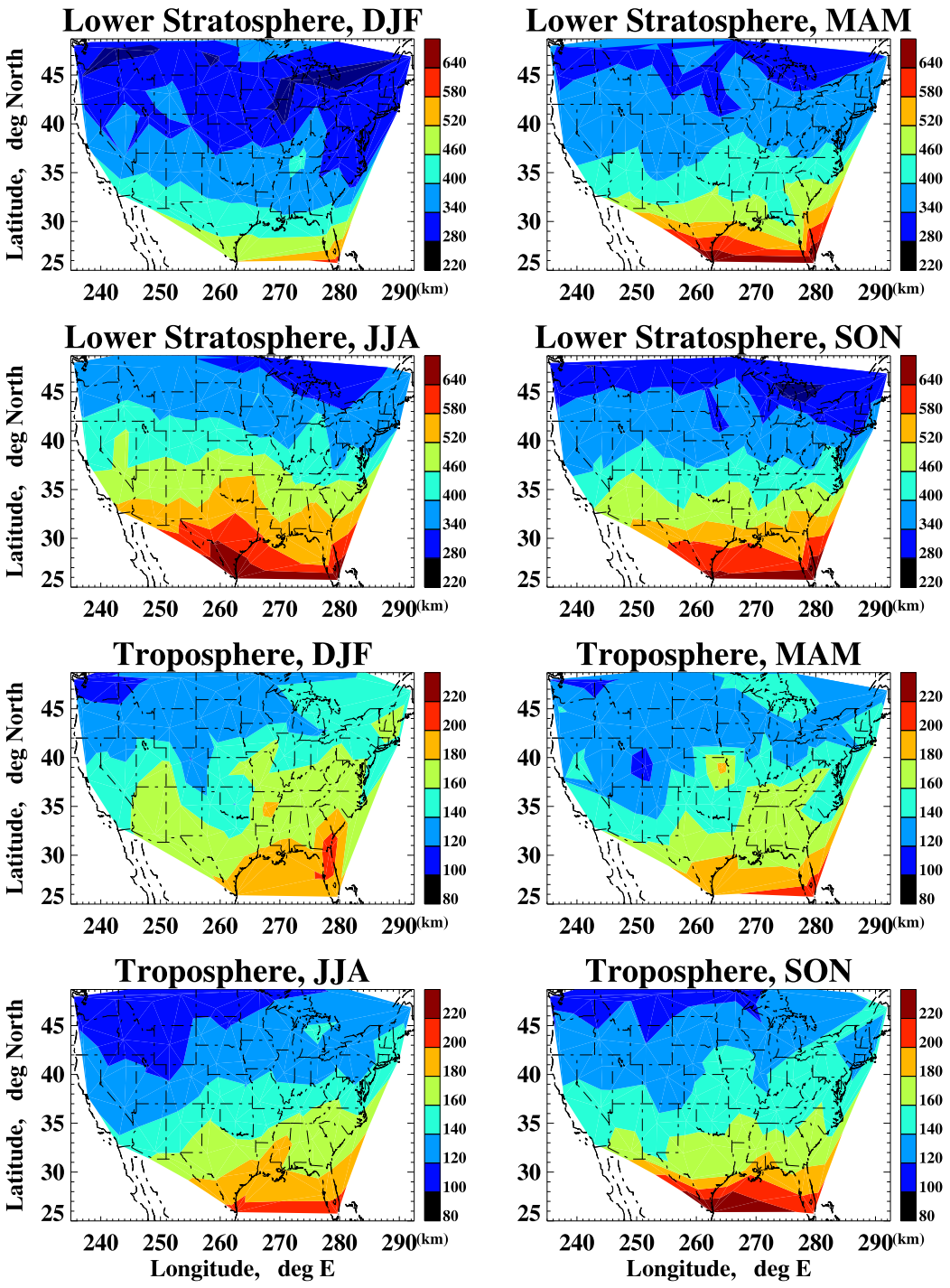

Fig. 4: Same as Fig. 2 but for the dominant horizontal wavelength $\overline{\lambda}_h$. The contour interval is 60 km for the lower stratosphere and 20 km for the troposphere.

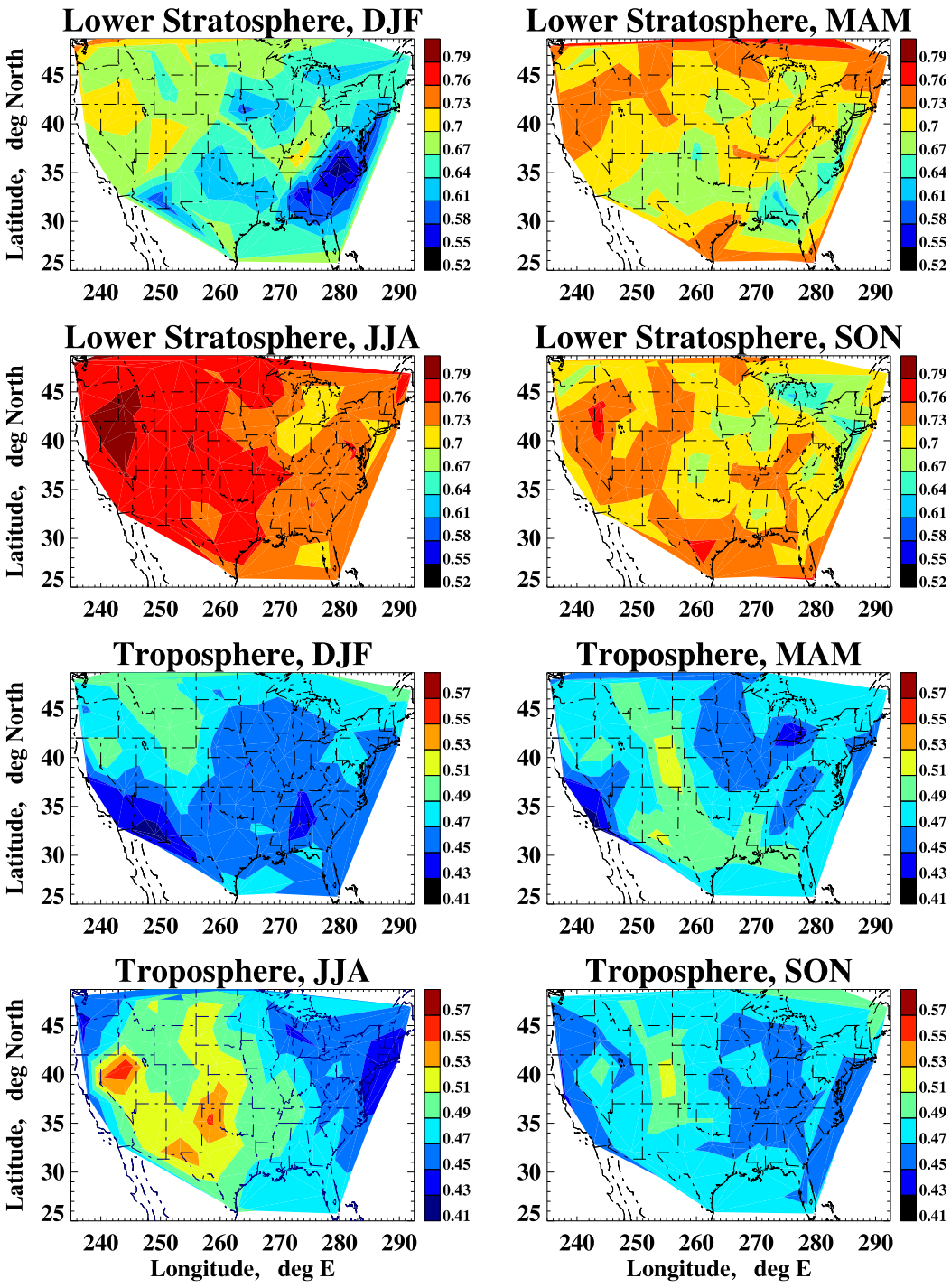

Fig. 5: Same as Fig. 2 but for the fraction of upward energy propagation. The contour interval is 0.03 for the lower stratosphere and 0.02 for the troposphere.

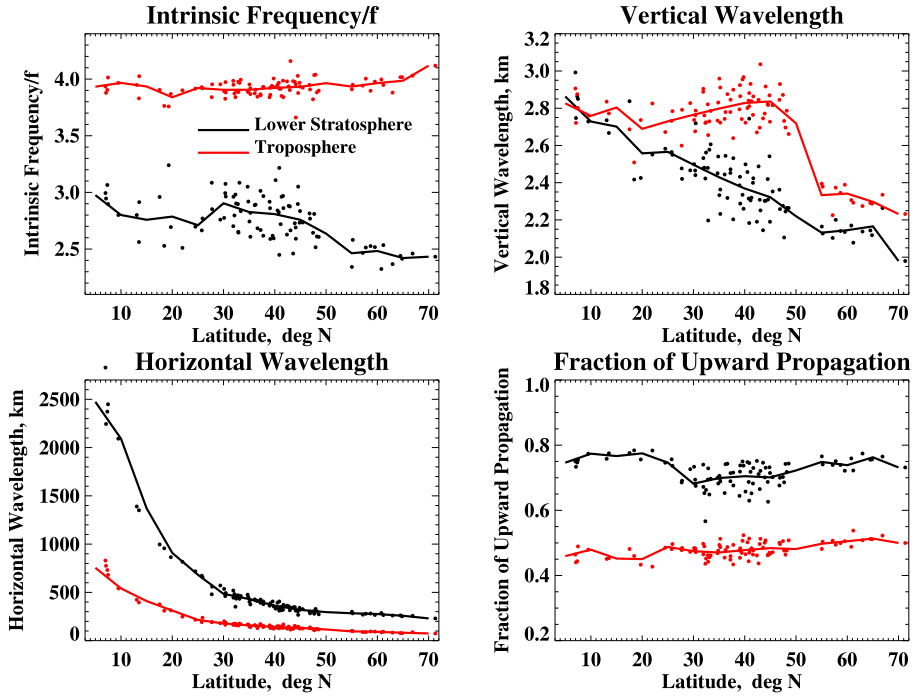

Fig. 6: Five-year (1998-2002) averaged $\hat{\omega}/f$, $\overline{\lambda}_z$, $\overline{\lambda}_h$, and fractions of upward propagation as functions of latitude in the troposphere (red dots) and lower stratosphere (black dots). The red and black solid lines are the latitudinal binned results (with a bin size of 5°) for the troposphere and lower stratosphere, respectively.

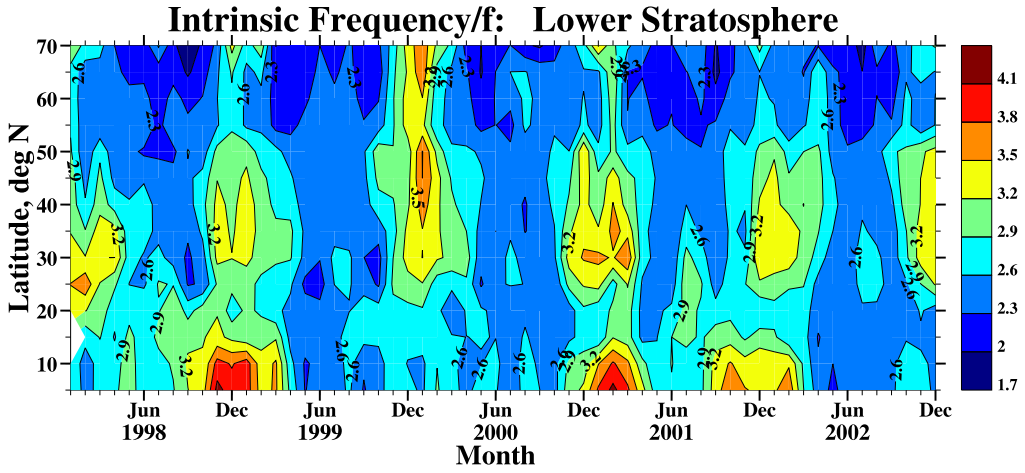

Fig. 7: Month-latitude contour of monthly and zonally averaged $\hat{\omega}/f$ in the lower stratosphere. The contour interval is 0.3. See text for details.

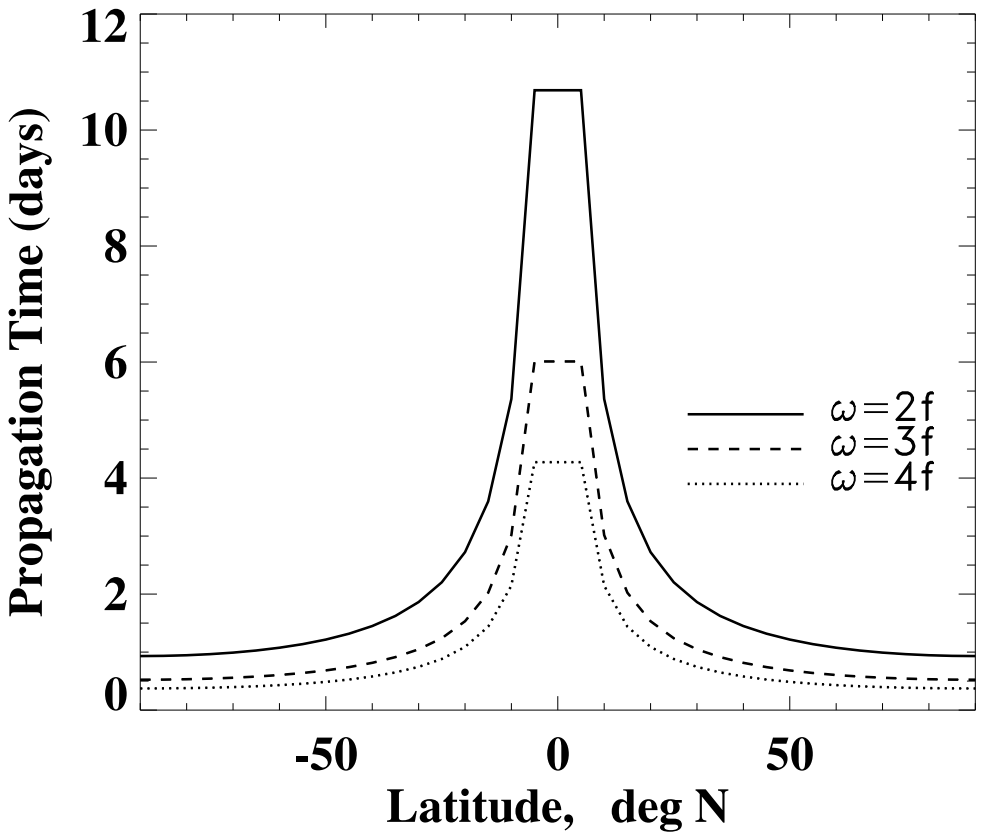

Fig. 8: Propagation time (in days) versus latitude for different intrinsic frequencies. The propagation time is the time it would take a wave of a given frequency and a vertical wavelength of 2.5 km to travel vertically through a 7-km-deep layer in the lower stratosphere.

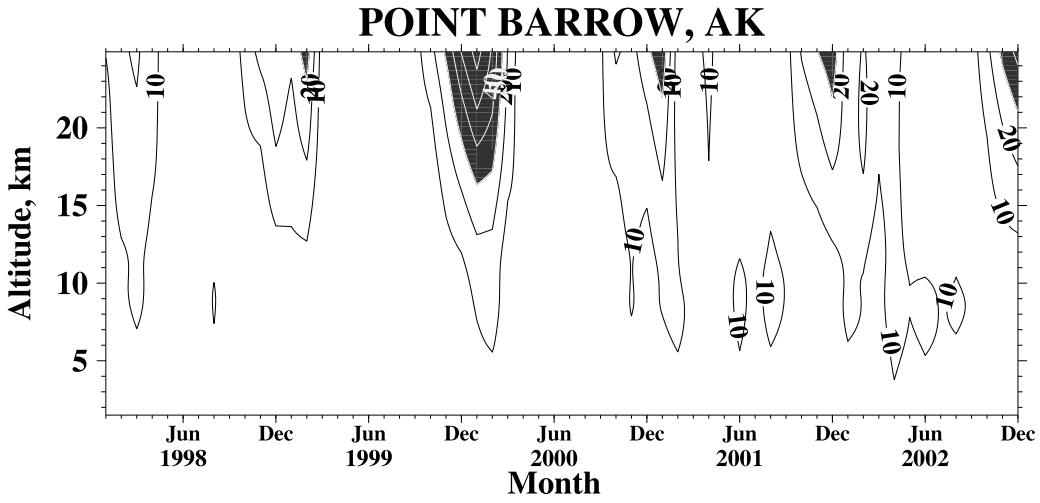

Fig. 9: Month-altitude contour of the monthly mean background wind speed over Point Barrow, AK (71.3°N, 203.2°E) (from U.S. radiosondes). The contour interval is 10 ms^{-1}. The part where the wind speed exceeds 30 ms^{-1} is shaded.

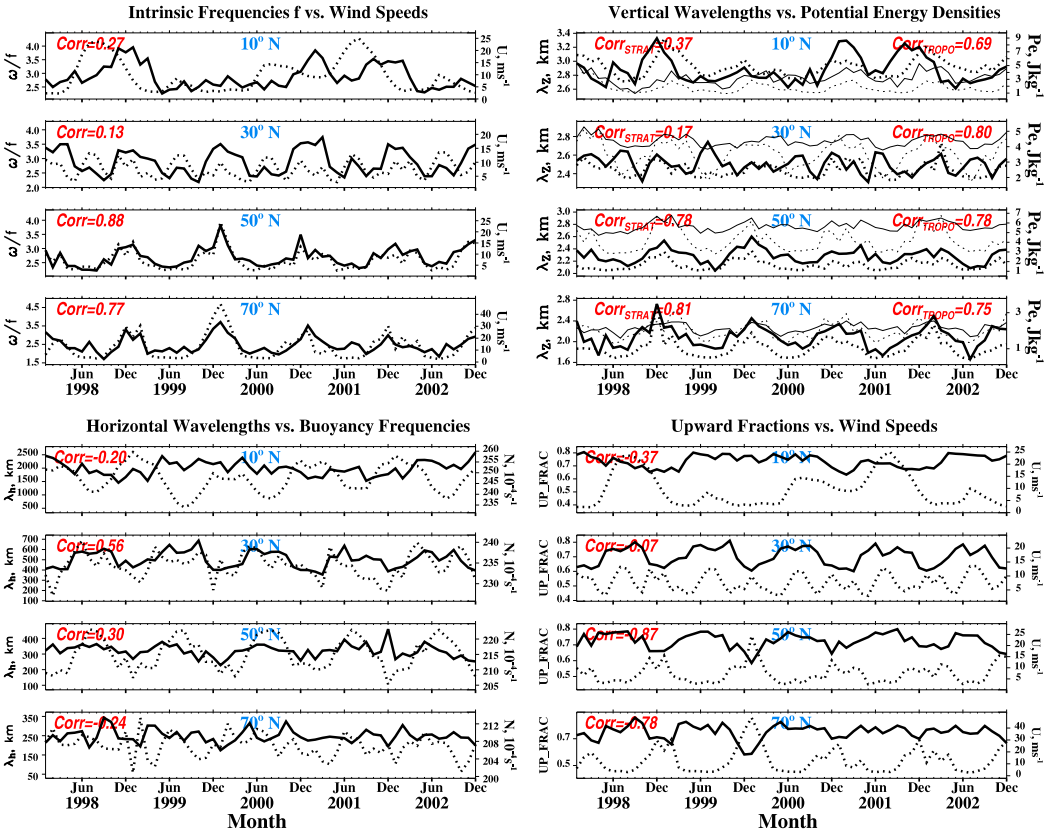

Fig. 10: Monthly time series of the monthly and zonally averaged $\hat{\omega}/f$ (thick solid lines) vs. wind speeds (thick dotted lines), $\overline{\lambda}_z$ (thick solid lines) vs. P_e (thick dotted lines), $\overline{\lambda}_h$ (thick solid lines) vs. Brunt-Väisälä frequencies (thick dotted lines), and fractions of upward propagation (thick solid lines) vs. wind speeds (thick dotted lines) in the lower stratosphere at different latitudes ($10^\circ - 70^\circ$N). The tropospheric $\overline{\lambda}_z$ (thin solid lines) vs. P_e (thin dotted lines) are also shown. See text for details.

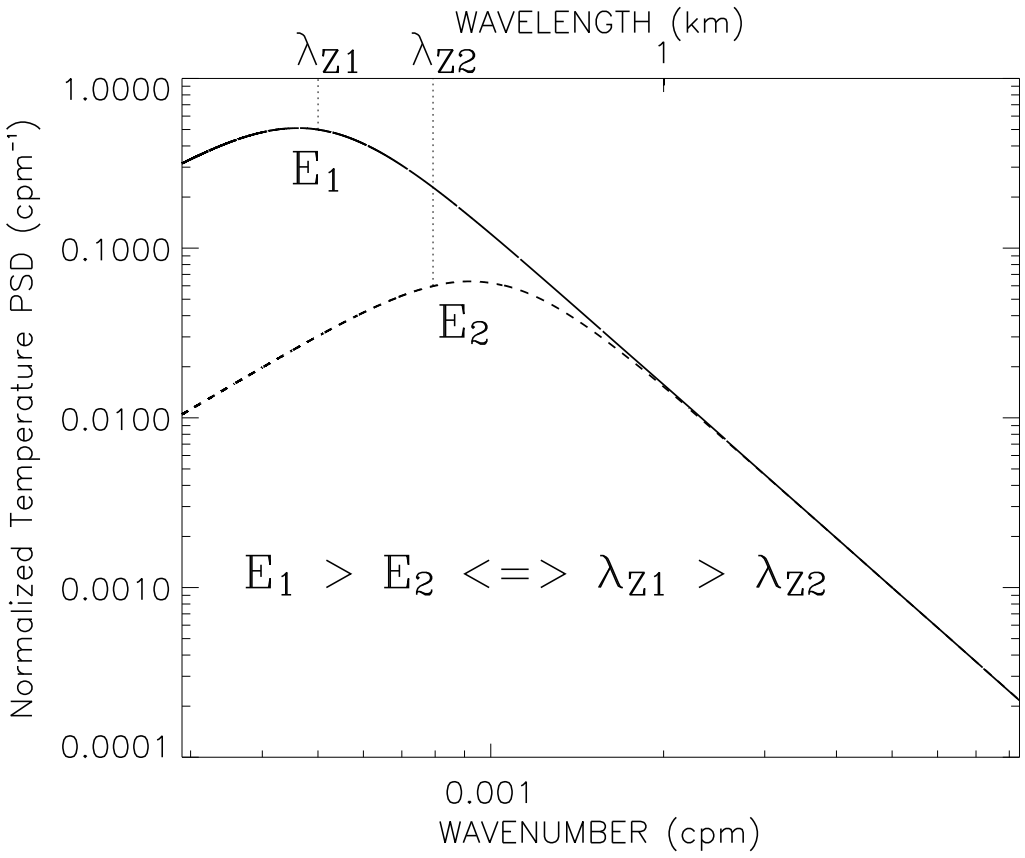

Fig. 11: Schematic showing vertical wavenumber power spectra of gravity wave perturbations with variances of E_1 and E_2, respectively, in energy-conserved form.

Table 1: The WBAN (Weather-Bureau-Army-Navy) ID numbers, station names, states, latitudes (deg N), and longitudes (deg E) of all the U.S. high vertical resolution radiosonde stations.

Station	**Lat**	**Lon**	**Station**	**Lat**	**Lon**
Pago Pago Intl Arpt, 99	-14.33	189.280	Sterling(Wash Dulles), VA	38.98	282.530
Ponape Island, 99	6.97	158.220	Topeka, KS	39.07	264.380
Majuro/Marshall Isl, 99	7.08	171.380	Grand Junction, CO	39.12	251.470
Koror/Palau IsLand, 99	7.33	134.480	Wilmington, OH	39.42	276.180
Truk Intl/Moen Isl, 99	7.47	151.850	Reno, NV	39.57	240.200
Yap Island, 99	9.48	138.080	Denver/Stapleton Arpt, CO	39.77	255.120
Seawell Apt, 99	13.07	300.500	Lincoln-Logan County Ap, IL	40.15	270.670
******, **[a]	13.5	144.800	Pittsburgh/Moon Township, PA	40.53	279.770
Guam, Mariana Is, 99	13.55	144.830	Salt Lake City, UT	40.77	248.030
Belize, 99	17.53	271.700	Elko, NV	40.87	244.270
San Juan/Isla Verde, PR	18.43	294.000	Brookhaven, NY	40.87	287.130
Grand Cayman, 99	19.30	278.630	North Platte, NE	41.13	259.320
Hilo, HI	19.72	204.930	Omaha/Valley, NE	41.32	263.630
Lihue/Kauai, HI	21.98	200.650	Davenport Municipal Ap, IA	41.60	269.430
******, **[b]	24.50	278.200	Chatham, MA	41.67	290.030
Miami/FL Intl Univ, FL	25.75	279.620	Medford, OR	42.37	237.130
Brownsville, TX	25.90	262.570	Detroit/Pontiac, MI	42.70	276.530
Tampa Bay/Ruskin, FL	27.70	277.600	Buffalo/Grtr Arpt, NY	42.93	281.270
Corpus Christi, TX	27.77	262.500	Riverton, WY	43.06	251.530
Del Rio, TX	29.37	259.080	Boise, ID	43.57	243.780
Lake Charles, LA	30.12	266.780	Gray, ME	43.89	289.750
Slidell, LA	30.33	270.180	Rapid City, SD	44.07	256.790
Tallahasee, FL	30.38	275.630	Green Bay, WI	44.48	271.870
Jacksonville, FL	30.43	278.300	Gaylord / Alpena, MI	44.55	275.570
Santa Teresa, NM	31.90	253.300	Minneapolis, MN	44.83	266.450
Midland, TX	31.93	257.800	Salem, OR	44.92	236.980
Tuscon, AZ	32.12	249.070	Aberdeen, SD	45.45	261.580
Jackson/Thompson Fld, MS	32.32	269.930	Bismarck, ND	46.77	259.250
Shreveport Regional Ap, LA	32.45	266.170	Caribou, ME	46.87	291.980
Ft Worth, TX	32.80	262.700	Great Falls, MT	47.45	248.620
Miramar Nas, CA	32.87	242.850	Spokane Intnl Apt, WA	47.68	242.370
Charleston, SC	32.90	279.970	Quillayute, WA	47.95	235.450
Birmingham (Shelby Apt), AL	33.10	273.300	Glasgow, MT	48.20	253.380
Peachtree City, GA	33.35	275.440	International Falls, MN	48.57	266.620
Morehead City/Newport, NC	34.70	283.200	Annette Island, AK	55.03	228.430
N Little Rock, AR	34.83	267.730	Cold Bay, AK	55.20	197.280
Albuquerque, NM	35.05	253.380	St Paul Island, AK	57.15	189.780
Norman, OK	35.23	262.530	Kodiak, AK	57.75	207.520
Amarillo, TX	35.23	258.300	King Salmon, AK	58.68	203.350
Flagstaff/Bellemt(Army), AZ	35.23	248.180	Yakutat, AK	59.52	220.330
Greensboro, NC	36.08	280.050	Bethel, AK	60.78	198.200
Nashville, TN	36.25	273.430	Anchorage Iap/Pt. Campbe, AK	61.17	209.980
Desert Rock/Mercury, NV	36.62	243.980	Mcgrath, AK	62.97	204.380
Roanoke/Blacksburg, VA	37.20	279.590	Nome Ap, AK	64.50	194.570
Springfield Regional Ap, MO	37.23	266.600	Fairbanks, AK	64.82	212.130
Oakland Int Ap, CA	37.75	237.780	Kotzebue, AK	66.87	197.370
Dodge City, KS	37.77	260.030	Point Barrow, AK	71.30	203.220

[a]The corresponding WBAN number is 12850.
[b]The corresponding WBAN number is 41406.